Low-Lying Excited States of Light-Harvesting System II in Purple Bacteria

Man-Fai Ng, Yang Zhao, and Guan-Hua Chen*

Department of Chemistry, University of Hong Kong, Hong Kong, P. R. China

Received: February 7, 2003; In Final Form: April 29, 2003

The light-harvesting system II (LH2) from *Rhodospirillum (Rs.) molischianum* is a two-ring circular aggregate composed of eight weakly coupled bacteriochlorophylls-a (BChls-a) in the B800 ring and sixteen strongly coupled BChls-a in the B850 ring. The linear-scaling localized-density-matrix (LDM) method has been implemented at the INDO/S level to probe the electronic structures of monomers, dimers, trimers, pentamers, and entire rings of BChls. The low-lying excited states of a B850 ring are found to fit extremely well with a Frenkel exciton model with long-range dipolar interactions. More importantly, the nearest neighboring BChls-a exciton coupling constants on a B850 ring are found to be close to those evaluated directly from dimers, and thus, an existing discrepancy between calculated results of dimers and B850 rings has been resolved. In addition, solvent effects are simulated and the results are compared to the experimental findings.

I. Introduction

The basic energy source for virtually all organisms is photosynthesis by which green plants and other organisms use the energy of light to convert carbon dioxide and water into the simple sugar glucose. To better capture sunlight, photosynthetic systems have developed various antenna systems that contain aggregates of chlorophylls, bacteriochlorophylls (BChls), or other chromophores. The structures of the light-harvesting apparatus in purple bacteria, such as *Rhodopseudomonas (Rps.) acidophila*[1] and *Rhodospirillum (Rs.) molischianum*,[2] have been resolved recently by X-ray crystallography. The photosynthetic unit (PSU) in these purple bacteria is generally composed of light-harvesting aggregates of bacteriochlorophyll (LH1 and LH2), carotenoids, and a reaction center (RC). The LH1 (B875) aggregate encircles the reaction center whereas the LH2 aggregate (B800 and B850) forms a peripheral network of pigment−proteon complexes located next to the LH1 aggregate. The carotenoid found in *Rs. molischianum* is Lycopene (Lyc), which plays an important role in structure stabilization and in preventing the formation of harmful singlet oxygen.[3] Sunlight is harvested by the LH2 and carotenoids, and the energy will be transferred to the LH1, and finally to the RC. This efficient energy transfer process has drawn much theoretical and experimental interest.

Excitation transfer can arise from two mechanisms in photosynthetic antenna systems, known as the Förster incoherent hopping (Markovian)[4,5] and the coherent exciton migration.[6] In the former case, the excitation is localized, i.e., the exciton resides on one or a few BChls-a, whereas in the latter case the exciton is coherently delocalized over a large number of BChls-a or the entire ring. Qualitatively speaking, the size of the excitonic coherence is determined by the ratio of the nearest-neighbor coupling constant to the energy disorder.[7] The energy disorder can either be static (spectral inhomogeneities) or dynamic (electron−phonon interactions).[8−10] If the energy disorder is much larger than the exciton coupling constants between adjacent BChls-a, Förster incoherent hopping is thus dominant. On the contrary, strong intermolecular interactions between next-nearest neighbor (denoted as J) would result in more significant delocalization of the excitation, and transfer via coherent exciton migration is then dominant.

There are many experimental and theoretical studies in determining the exciton size in LH2. Various results where the exciton size ranges from a few pigment molecules[11−16] to the entire ring[17] have been reported. In particular, pump−probe spectroscopy predicted a coherence length covering a few BChl molecules[18,19] and the experiment studying the superradiance of the B850 ring at room temperature resulted in a coherence length of about 3 pigments.[14] A transient absorption study[17] showed the exciton is delocalized in the entire B850 ring. Theoretical studies such as the Redfield theory and the path integral formulation estimated a delocalization length of 2−4 pigments.[15,20,21] The static energy disorder has been measured directly from the absorption line widths in hole-burning experiments. It was concluded that static energy disorder varies between 200 and 500 cm^{-1}. Dynamic disorder was estimated to be between 100 and 500 cm^{-1}. The interchromophore coupling constants play an important role in the energy transfer process. Their values are difficult to measure experimentally and, therefore, need to be evaluated by quantum mechanical methods.

The LH2 complex of *Rs. molischianum* is built from $\alpha\beta$-heterodimers forming an eight-unit circular aggregate with C_8 symmetry. Each unit contains a pair of α and β polypeptides, three BChls-a and one carotenoid. The polypeptides bind to the BChls-a and the carotenoid noncovalently. The BChls-a form two rings, named according to their corresponding absorption maxima at 800 and 850 nm, as the B800 and B850 rings. The B850 ring consists of sixteen tightly positioned BChls-a, and the B800 ring, of eight loosely spaced BChls-a. Hence, the crystal structure of *Rs. molischianum* is an octamer. A projection of the B850 and B800 aggregates onto the ring-plane is shown in Figure 1. By a measurement based on the central Mg atom in the porphin ring, the radius of the B850 ring is approximately 23 Å, and that of the B800 ring, 28 Å. The geometries of the BChls-a within an $\alpha\beta$-heterodimer unit are slightly different. For the B800 ring it contains eight units of BChls-a with about 22 Å between neighboring Mg atoms. For the B850 ring, the BChls-a bound to the α-apropotein and β-apropotein are labeled

10.1021/jp034320r CCC: $25.00
Published on Web 08/09/2003

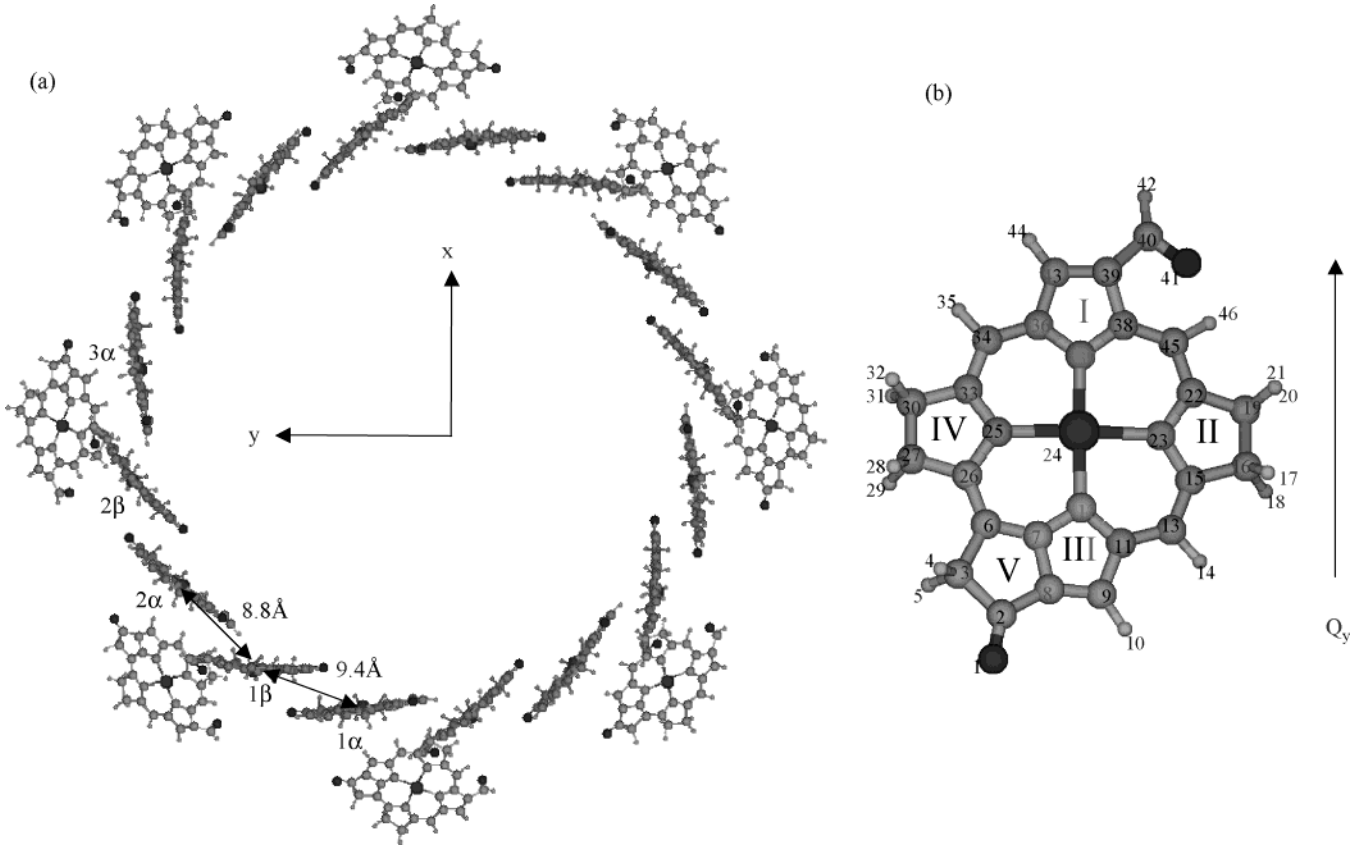

Figure 1. (a) Labeling scheme of LH2. Note that the Mg-to-Mg distances for the 1α−1β dimer, 1β−2α dimer, 1α−2α dimer, 1β−2β dimer, 1α−2β dimer and 1β−3α dimer are 9.4, 8.8, 17.4, 18.0, 26.0, and 25.5 Å, respectively. The outer ring is the B800 ring and the inner ring is the B850 ring. (b) The truncated bacteriochlorophyll-a (BChl-a), which contains 46 atoms.

as α-BChl-a and β-BChl-a, respectively, as shown in Figure 1a. The Mg-to-Mg distance is about 9.36 Å for the 1α−1β dimer, and about 8.78 Å for the 1β−2α dimer, which can be compared with the center-to-center values in ref 7. Note that the Mg-to-Mg distances in the intra- and interdimers were found to vary for different crystal structure data. It can be attributed to the fact that the proteins form different conformers upon crystallization and the reported distances in ref 2 are the average among the conformers. Hence, the crystalline Mg-to-Mg distances are also slightly different from those in in-situ LH2. In our calculations, we adopt the crystal data without any modifications to generate the B850 and B800 rings according to C_8 symmetry and the known geometrical parameters.[2]

Within the B850 ring, the BChls-a are closely packed and the inter-BChl-a is comparable to the chromophore size (9 Å). As the chromophore is mainly located on the porphin ring, the phytyl tail and some alkyl groups are eliminated during the calculations. Each BChl-a is truncated to 46 indexed atoms (cf. Figure 1b). The total number of atoms for the B800 ring is then 368, and for the B850 ring, 736. In this paper we are mainly concerned with the low-energy absorption Q band of the BChl-a. The lowest two transitions for the BChl-a are the Q_y and Q_x transitions. The corresponding transition dipole moments lie along the two perpendicular directions[22,23] in the porphin ring as shown in Figure 1b. Several calculations were carried out for the LH2 from *Rs. molischianum*, and different calculated J values were reported. The collective-electronic-oscillator (CEO) method[24,25] was applied to calculate the dimeric coupling constants for the LH2. It was determined that two coupling constants, J_1 and J_2, are respectively 408 and 366 cm^{-1} (J_1 is denoted to be the 1α−1β coupling constant, and J_2, the 1β−2α coupling constant; see Figure 1a). Cory et al.[26] used a generalized Frenkel exciton model by including long-range dipolar interactions to describe the low-lying excitonic states. They carried out an INDO/S (intermediate neglect of differential overlap/spectroscopy) calculation at the configuration-interaction-singles (CIS) level on the entire B850 ring. The resulting energy levels were employed to determine the parameters in their Frenkel exciton model. Computational feasibility limited their configuration-interaction (CI) expansion to 4096 configurations for each of the A and B representations of the C_8 symmetry group, and 790 and 369 cm^{-1} were reported for J_1 and J_2, respectively. The same method was used previously by Hu et al.,[3] but with a CI expansion of 512 configurations for each symmetry class, and they reported 806 and 377 cm^{-1} for J_1 and J_2, respectively. Sundström et al.[7] used the point-dipole approximation (PDA) to calculate J_1 and J_2, which were found to be 339 and 336 cm^{-1}, respectively. All these studies were based on the crystal structure model[2] with C_8 symmetry, and no structural disorder was included.

The calculated values for J_1 and J_2 vary from 300 to 800 cm^{-1}, which implies that the energy transfer can either be via Förster hopping or via the exciton coherent migration. Most of these calculations were on monomers or dimers, except the calculation by Schulten, Zerner, and co-workers, which was on the entire B850 ring.[3,26] Apparent discrepancies between the calculated results from dimers and those from the entire B850 ring require further investigations. One possible cause is that long-range Coulombic interactions in the ring are absent in dimers. The long-range dipolar interactions may affect the exciton wave functions significantly. On the other hand, the truncation adopted in the INDO/S-CIS calculations[3,26] introduced the uncertainties in the results and might lead an overestimation

of J_1 and J_2.More accurate calculations on the entire B850 ring are thus desirable.

The linear-scaling localized-density-matrix (LDM) method has been developed to calculate the excited-state properties of large molecular systems. It has been employed to calculate the absorption spectra of polyacetylene oligomers[27−29] and carbon nanotubes.[30−32] In this paper we implement the LDM at the INDO/S level and employ the resulting INDO/S-LDM method to calculate the low-lying excited-state energies of LH2 aggregates in *Rs. molischianum*. The INDO/S method is well-suited for spectroscopy calculations on LH2.

The paper is organized as follows. In section II we describe the INDO/S-LDM method and the computational procedures. In section III the calculated absorption spectra of monomers, dimers, trimers, pentamers, and rings are presented. In section IV a special procedure is presented to evaluate the energies of low-lying dipole-forbidden excited states, and the resulting energy spectrum is given. In section V a least-squares fitting method is described for determining the parameters in the generalized Frenkel exciton model. The resulting values of J_1 and J_2 for different systems are given and analyzed. The solvent effects on monomers and the J coupling constants are determined in section VI. Conclusions are given in section VII.

II. Method

The INDO/S parameters used in these calculations are from ref 33 by Zerner et al. The geometry is based on the crystal structure of the *Rs. molischianum* complex,[2] obtained from the Protein Data Bank (PDB) of the Research Collaboratory for Structural Bioinformatics (RCSB) with the PDB identification code 1LGH. Hydrogen atoms are added using the Insight II software, and their coordinates are optimized with the semiempirical PM3[34] method. All other atoms are fixed at their crystal structure coordinates. The ZINDO method[35−37] is employed to generate the ground-state density matrices and Fock matrices. The INDO/S-LDM method is then employed to calculate the absorption spectra.

The INDO/S Hamiltonian[35−37] in the presence of an external field **E** reads

$$\hat{H} = \sum_{ab}\sum_{i\in a,j\in b} t_{ij}c_{ai}^{\dagger}c_{bj} + \frac{1}{2}\sum_{a}\sum_{ijmn} V_a^{ij,mn}c_{ai}^{\dagger}c_{am}^{\dagger}c_{an}c_{aj} + \frac{1}{2}\sum_{a\neq b}\sum_{i\in a,j\in b}\gamma_{ab}^{ij}c_{ai}^{\dagger}c_{ai}c_{bj}^{\dagger}c_{bj} - \mathbf{E}(t)\cdot\sum_{mn}\hat{\mathbf{P}}_{ab}^{mn}c_{am}^{\dagger}c_{bn} \quad (2.1)$$

where $c_{ai}^{\dagger}$ (c_{bj}) is the creation (annihilation) operator for an electron at a localized atomic spin−orbital i (j) on atom a (b). $V_a^{ij,mn}$ is the on-site repulsion, and γ_{ab}^{ij} stands for the two-center repulsion. The one-electron hopping integral t_{ij} may be expressed as

$$t_{ij} = \left\langle \chi_a^i \right| -\frac{1}{2}\nabla_{\mathbf{r}}^2 + U(\mathbf{r}) \left| \chi_b^j \right\rangle \quad (2.2)$$

where χ_i (χ_j) is the ith (jth) atomic orbital on atom a (b), and $U(\mathbf{r})$ is the one-electron potential. The second and the third terms in eq 2.1 represent the effective electron−electron Coulombic interaction. The last term describes the interaction between the valence electrons and an external electric field $\mathbf{E}(t)$, and $\hat{\mathbf{P}}$ is the molecular dipole moment operator. $\mathbf{P}_{ab}^{ij}$ is calculated by $\langle\chi_a^i|\hat{\mathbf{P}}|\chi_b^j\rangle$, neglecting the diatomic overlap. Taking into account the linear response only, the reduced single-electron density matrix $\rho(t)$ may be written as $\rho(t) = \rho^{(0)} + \delta\rho$, where $\rho^{(0)}$ is the ground-state reduced density matrix, and $\delta\rho$ is the field-induced density matrix deviation. Similarly, the Fock matrix h can be decomposed into $h = h^{(0)} + \delta h$, where $h^{(0)}$ is the Fock matrix in the absence of the external field:

$$h_{ab}^{(0)mn} = t_{ab}^{mn} + \delta_{ab}\left[2\sum_{ij\in a}\left(V_a^{mn,ij}\rho_{aa}^{(0)ij} - \frac{1}{2}V_a^{mi,nj}\rho_{aa}^{(0)ij}\right)\right] + \delta_{ab}\delta_{mn}\sum_{c\neq a}\sum_{l\in c}2\rho_{cc}^{(0)ll}\gamma_{ac}^{ml} - \rho_{ba}^{(0)nm}\gamma_{ab}^{mn} \quad (2.3)$$

And, similarly, the field-induced Fock matrix can be written as

$$\delta h_{ab}^{mn} = \delta_{ab}\left[2\sum_{ij\in a}\left(V_a^{mn,ij}\delta\rho_{aa}^{(0)ij} - \frac{1}{2}V_a^{mi,nj}\delta\rho_{aa}^{(0)ij}\right)\right] + \delta_{ab}\delta_{mn}\sum_{c\neq a}\sum_{l\in c}2\delta\rho_{cc}^{ll}\gamma_{ac}^{ml} - \delta\rho_{ba}^{nm}\gamma_{ab}^{mn} \quad (2.4)$$

The single-electron density matrix follows the equation of motion:

$$\left(i\hbar\frac{\mathrm{d}}{\mathrm{d}t} + \gamma\right)\delta\rho(t) = [h^{(0)}, \delta\rho(t)] + [\delta h(t), \rho^{(0)}] - \mathbf{E}(t)\cdot[\mathbf{P}, \rho^{(0)}] \quad (2.5)$$

where γ is the dephasing constant. In computing the excited-state properties, the following approximations are employed to achieve linear-scaling of computational time with the number of orbitals[30,38,39]

$$\rho_{ab}^{(0)mn} = 0 \quad \text{if} \quad r_{ab} > l_0$$

$$\delta\rho_{ab}^{mn} = 0 \quad \text{if} \quad r_{ab} > l_1$$

where r_{ab} are the distances between two atoms a and b and l_0 and l_1 are the density-matrix truncation length scales, or the cutoff lengths. In the calculations on the LH2 here, the truncation lengths l_0 and l_1 are set to be the same.

III. Absorption Spectrum and Dipole Induced Excited States

A. Monomers. For monomers and dimers no density-matrix truncations are needed in the LDM calculations. The absorption spectra of three types of BChl-a monomers, namely, B800 BChl-a, α-BChl-a, and β-BChl-a, are shown in Figure 2. The Q_y (Q_x) transition energies for B800 BChl-a, α-BChl-a, and β-BChl-a are 1.18 eV (2.27 eV), 1.17 eV (2.16 eV), and 1.15 eV (1.98 eV), respectively. The Q_y transition frequencies for the three different monomers fall within 0.03 eV; see Table 1.

The Q_y transition in a BChl-a carries a strong oscillator strength in contrast to a porphin ring where the Q transitions are only weakly dipole allowed.[40] In a porphin ring, the absorption peaks inside the Soret B band (spanning about 3 eV) carry the strongest oscillator strength whereas the Q band carries a very small oscillator strength experimentally.[41] It is because the free-base porphin adopts a D_{2h} symmetry, and so does the π conjugation. The LDM method and other theoretical studies such as CEO, RPA, SAC−CI, and STEOM-CCSD[40,42−44] also give similar conclusions. In a BChl-a, in addition to an extra ring V lying next to pyrrole III and the C═O groups (cf. Figure 1b), electron densities are significantly weakened at rings II and IV as compared with those at rings I and III because rings II and IV do not participate in the π conjugation in the chromophore part. As a result, the Q_y transition shows a significant increase of the oscillator strength whereas the Q_x transition in BChl-a is rendered weakly dipole-allowed. Our resulting energies for Q_y

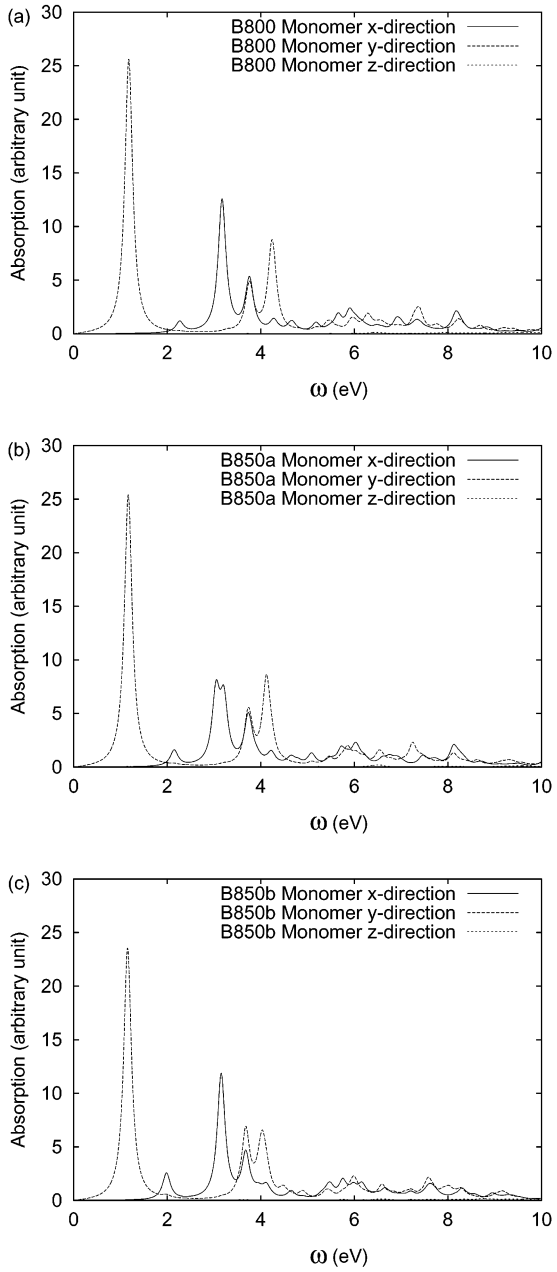

Figure 2. Absorption spectrum of (a) B800 BChl-a, (b) α-BChl-a, and (c) β-BChl-a.

TABLE 1: Q_y and Q_x Excitation Energies for Three Different Monomers in the LH2 System[a]

monomer	Q_y (eV)	Q_x (eV)
B800 BChl-a	1.18 (1.38)	2.27 (2.32)
α-BChl-a	1.17 (1.42)	2.16 (2.15)
β-BChl-a	1.15 (1.44)	1.98 (1.96)
experimental results	1.6	2.16

[a] Values in parentheses include solvent effects.

(1.17 eV) and Q_x (2.15 eV) are in agreement with those obtained by Tretiak et al.[24,25] Both methods are based on the TDHF approximation and the INDO/S model.

B. Dimers and Protein/Carotenoid Environment. Influence of the protein environment and energetics and dynamics of carotenoids in various species of purple bacteria attracted much experimental and theoretical interest.[45−47] Proteins in LH2 are generally believed to provide only structural support and do not significantly affect the electronic structures. Carotenoids absorb light at about 2.5 eV and, therefore do not intervene in the low-lying excitations. These issues are examined by our calculations. In Figures 3a,b we compared the absorption spectra of isolated 1α−1β dimer, of 1α−1β dimer with the protein moiety, and of 1α−1β dimer with the protein moiety and carotenoid. The corresponding structure is shown in Figure 4. To facilitate truncations in the computation, the system will be divided into subsystems as follows. For dimers, each BChl-a represents one subsystem. For the proteins, each amino acid segment represents one subsystem. For the carotenoid, the whole chain is divided into two parts; hence, the part far away from the dimer contains 39 atoms and the part closer to the dimer contains 57 atoms. For the latter two calculations, the α and β apoproteins are cut to retain a range of segments that are close to the dimer. Then, a cutoff length of 10 Å is applied in these two calculations so that each BChl-a would include another BChl-a and also some parts of the protein and the carotenoid in the calculation. We find that the Q_{y1} and Q_{y2} transitions are red-shifted insignificantly to nearly the same extent with the added protein environment (<0.01 eV), as shown in Figure 3b. This implies that proteins and carotenoids can be neglected for the Q band calculation.

Parts c and d of Figure 3 display the absorption spectra of the 1β−2α and 1α−1β dimers, respectively. Due to their different Mg-to-Mg distances and intermonomer angles, we obtain quite different absorption energies, Davydov splittings,[6,48] and intermonomer coupling energies. The absorption energies for Q_{y1} and Q_{y2} in the 1α−1β (1β−2α) dimer are 1.08 and 1.21 eV (1.09 and 1.21 eV), respectively (cf. Table 2). It follows that the electronic splitting for the 1α−1β (1β−2α) dimer is 0.13 eV (0.11 eV). These values are larger than those from ref 24 (0.10 and 0.09 eV for the 1α−1β dimer and 1β−2α dimer, respectively). The discrepancies may be attributed to different BChls-a truncation sizes. We take into account only 46 atoms for each BChl-a. Besides, the original INDO/S parametrization was based on a CI calculation with a truncated active space.[49] In the LDM method, the complete active space is considered and the calculated Q_y excitation in a BChl-a molecule using the original parametrization is blue-shifted to below 1 eV. The original parametrization may not reproduce the experimental spectral peaks well if a large active space is considered. Hence, we adopt the parameters of ref 33, which can reproduce much better measured spectral peaks of the Q_y and Q_x excitations in a BChl-a molecule. The main difference between these two sets of parameters is the bonding parameter (β), which is an empirical parameter (cf. refs 33 and 37). Despite the discrepancies, our results agree with ref 24 in that the 1α−1β dimer has a larger coupling constant due to their parallel arrangements despite a longer Mg-to-Mg distance.

C. Trimer, Pentamer, and Cutoff Length. To determine an appropriate cutoff length for calculations of the B800 and B850 rings, we have carried out calculations on trimers and pentamers with and without the cutoffs. In both calculations, each BChl-a represents one subsystem. For the B800 ring, we simply choose a cutoff length so that only the nearest-neighbors of BChls-a are included. As the Mg-to-Mg distance for the nearest BChl-a in the B800 ring is about 22 Å, a cutoff length of 30 Å is taken for the B800 ring. On the other hand, for the B850 ring, the choice of the cutoff length has been examined by the trimer and pentamer calculations.

Figure 5 compares the absorption spectra of the trimer and the pentamer with and without cutoffs. The Q_y excitation energies are found to be the same for both the trimer and the pentamer with and without cutoffs (1.04 and 0.99 eV for the trimer and the pentamer, respectively; and the cutoff length is set to be 15 Å). Therefore, coherence between next-neighbor

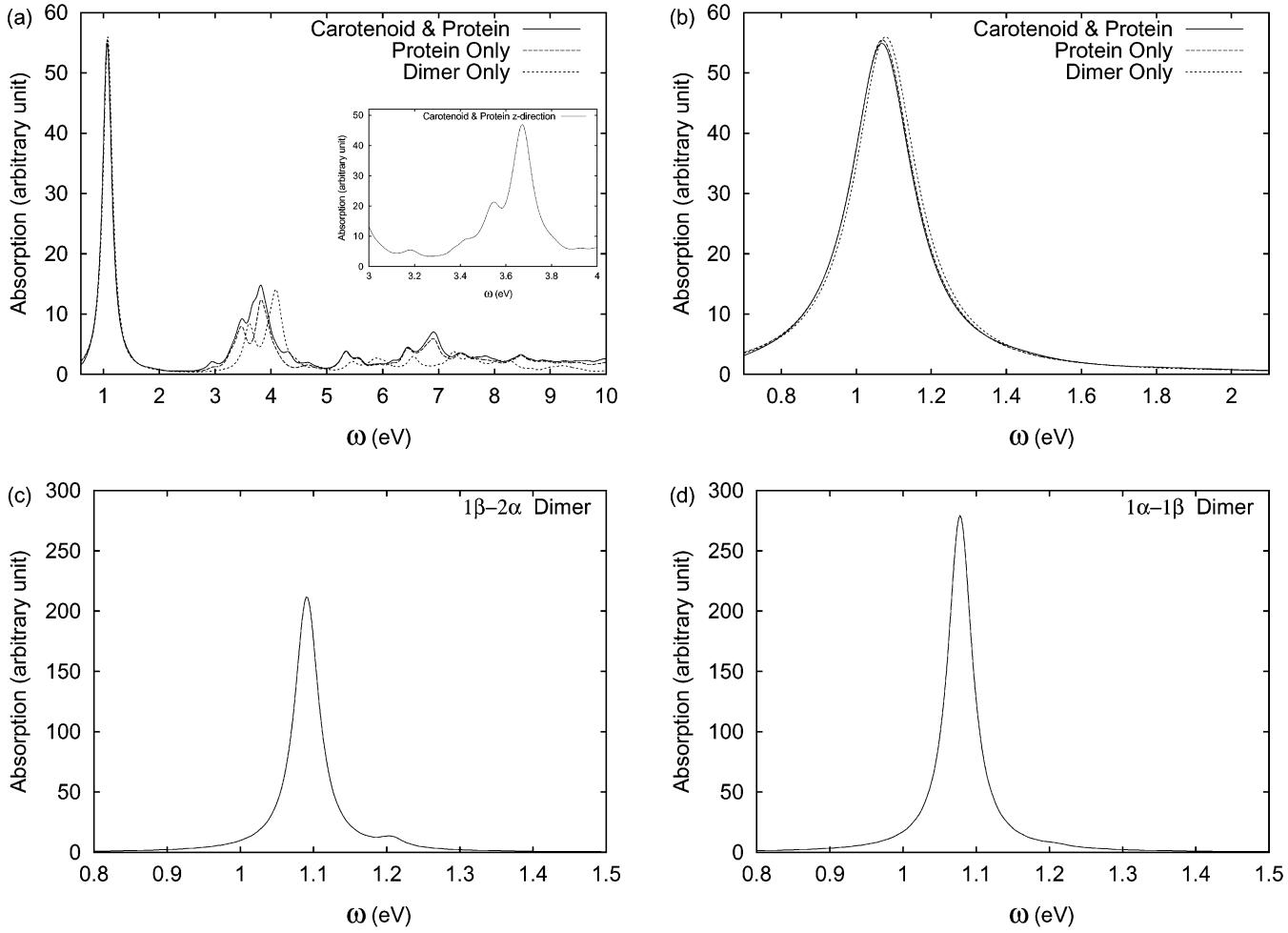

Figure 3. (a) and (b) compare three calculations on the 1α−1β dimer with and without a protein environment. (I) Dimer calculation with a protein environment and the carotenoid. (II) Dimer calculation with a protein environment only. (III) Dimer calculation only. Note that the Q_y excitation spectrum does not change significantly. The inset in (a) shows the absorption peak of carotenoid at about 3.6 eV. In (b), only an insignificant red shift of the Q_y transition is found with the protein environment included in the calculation. The absorption spectrum of (c) 1β−2α dimer and (d) 1α−1β dimer. The first Q_y transition splits into two levels with the Q_{y1} peak carrying most of the oscillator strength.

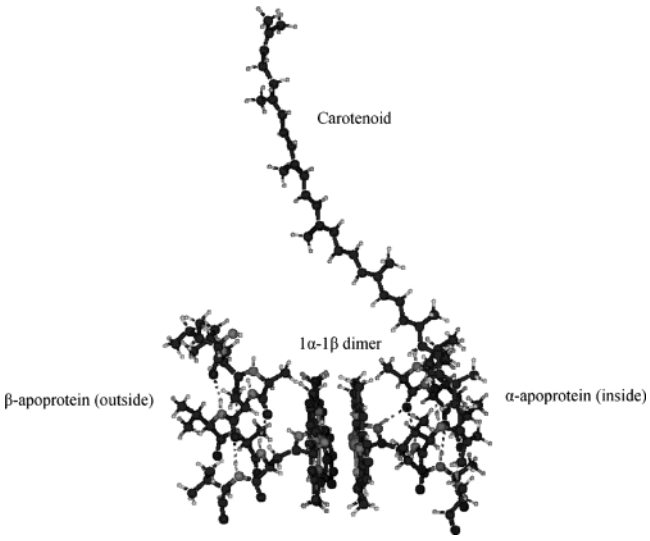

Figure 4. Structure of the 1α−1β dimer with surrounding proteins and the carotenoid. Parts of the proteins within 10 Å are included in the calculation.

BChls-a is included in the density matrix, which is truncated by the 15 Å cutoff length. The absorption spectra from calculations with and without cutoffs are nearly identical. Small differences are found for the Q_x transition and the peaks at higher energies. Therefore, we conclude that the Q_y excitation is mainly confined to one to two BChls-a, and the cutoff length of 15 Å we adopted is adequate for calculating Q_y and Q_x transitions, and is thus used in the calculation of B850 rings. More importantly, this shows that the electron−hole distances of Q_y excitons are confined to, at most, two BChls-a.

D. B800 and B850 Rings. Figure 6a displays the absorption spectrum of the B800 ring with an applied external field along an in-plane direction. The Q_y and Q_x excitation energies that carry the strongest oscillator strengths are 1.16 and 2.26 eV, respectively. If the external electric field is applied in the *z*-direction (see the inset in Figure 6a), a peak at about 1.15 eV is found with a small oscillator strength (the lowest energy state for the B800 ring). This can be explained by the fact that the transition dipole for each BChl-a is not entirely in the plane of the B800 ring. A small component of *y*-direction dipole can be induced when the electric field is applied in the *z*-direction. As compared with the B800 BChl-a monomer absorption spectrum, the energy of the Q_y transition is slightly red-shifted by about 0.02 eV. This can be explained by large spatial separations between individual monomers in the B800 ring.

Figure 6b shows the absorption spectrum of the B850 ring with an applied external field lying in the plane of the B850 ring. The spectrum for the B850 ring does not depend on the direction of the in-plane applied field, as will be explained in the next section. The optically allowed Q_y excitation in the B850

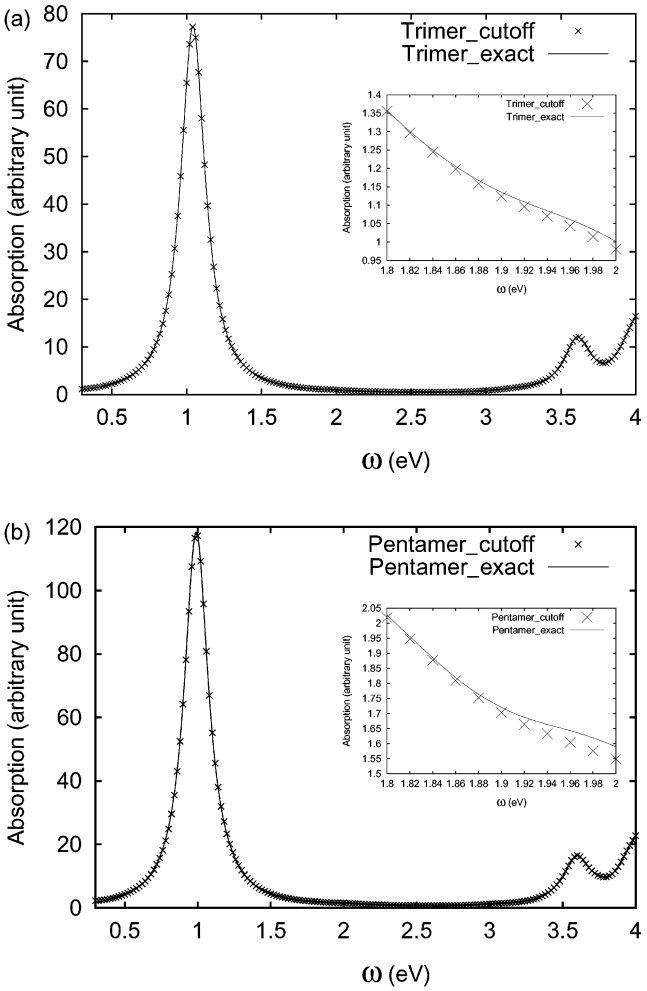

Figure 5. Absorption spectra of (a) a trimer calculation with and without density-matrix truncations (cutoff length = 15 Å). (b) Pentamer calculations with and without density-matrix truncations (cutoff length = 15 Å). The solid line is the exact calculation, and the crosses are the results calculated with density-matrix truncations in both (a) and (b). Calculations with and without cutoffs yield nearly identical results. The inset in each plot shows the difference betweent calculations with and without cutoffs in higher energies.

ring is found at 0.98 eV. However, this optically allowed state is not the lowest energy state in the B850 ring. The lowest energy state, which is symmetry forbidden (cf. section IV), is calculated to be at 0.93 eV consistent with a trend of red shift as one goes from a monomer to a dimer, a trimer, and a pentamer (1.17, 1.08, 1.04, and 0.99 eV, respectively). Discussions of the selection rule will be given in the next section.

Figure 6c shows the absorption spectrum of the B850 ring calculated with the density matrices truncated to be within one single monomer. With the electron−hole pair confined within one monomer, the dipole allowed Q_y excitation now has an energy of 1.03 eV, which is blue-shifted by about 0.05 eV from that in the spectrum of Figure 6b. This implies that the electron−hole pair actually spreads to neighboring BChls-a. We therefore conclude that the Frenkel exciton model for this system is reasonably good but may require some corrections.

IV. Dipole Forbidden Excited States

The B850 ring made of 16 BChls-a is of C_8 symmetry and there are totally 16 energy levels. Due to the symmetry and the dimeric nature, the energy levels split into 2 bands, one band is

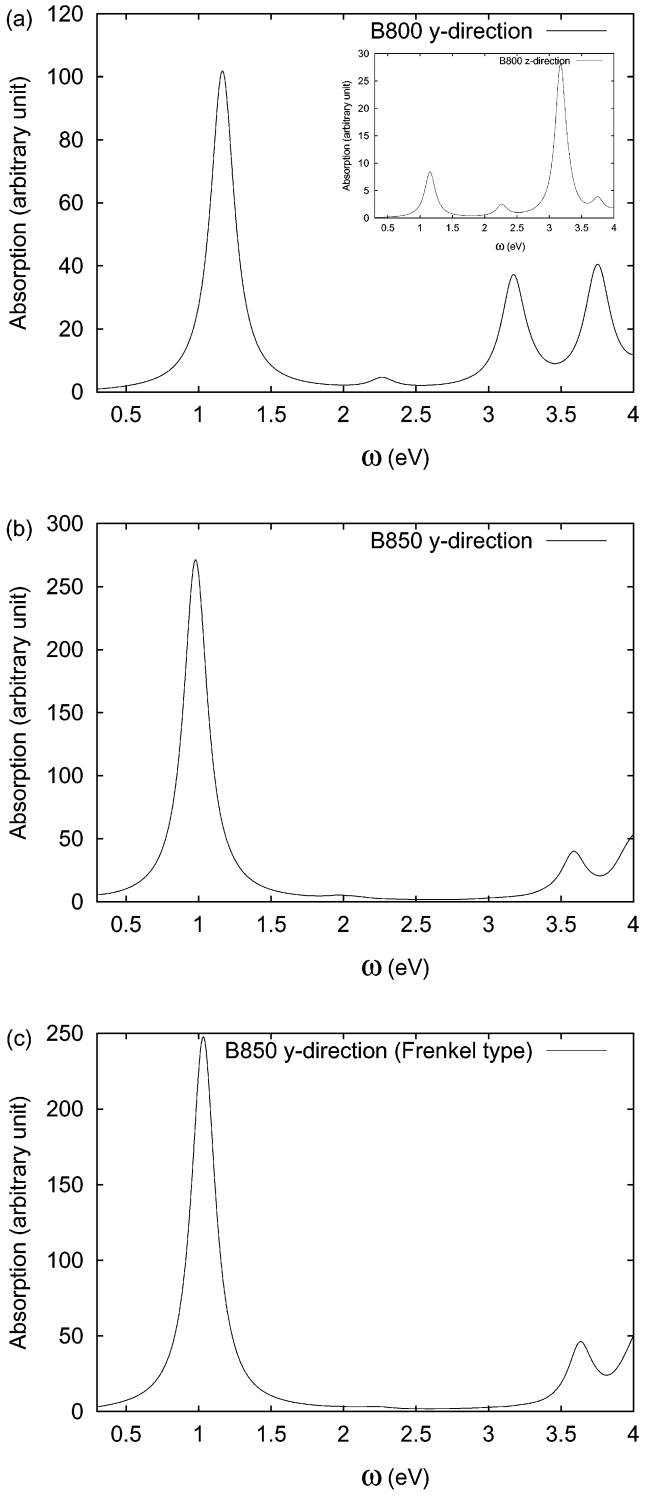

Figure 6. Absorption spectrum of (a) the B800 ring, (b) the B850 ring with a cutoff length of 15 Å, and (c) the B850 ring with a cutoff length of 1 Å. The corresponding directions of transition dipole are depicted in Figure 1. The inset in (a) shows the *z*-direction excitation of the B800 ring.

of higher energy and another is lower. Each band contains 5 energy levels, among which 3 of them are doubly degenerate. The doubly degenerate optically allowed energy states in the lower band have been resolved (cf. Figure 6b). To investigate the rest of 14 dipole forbidden energy levels, a fictitious external field is employed to calculate the dipole forbidden excited states. The details of the selection rules for all these energy states are discussed as follows.

Without loss of generality, we put aside dimerization in the B850 ring in this section and treat the B850 ring as a uniformly spaced ring of 16 monomers in discussing selection rules. The 16 eigenstates are labeled by their crystal momenta

$$k = 0, \qquad k = \pi, \qquad \text{and} \qquad k = \pm\frac{n\pi}{8}(n = 1, ..., 7) \quad (4.1)$$

The $k = 0$ and $k = \pi$ states are nondegenerate, and the rest of 14 states are doubly degenerate. The energy degeneracy at $k = \pm\pi/2$ is lifted upon dimerization.

The dipole-allowed excitations can only happen between the ground state and the excited states with crystal momenta $k = \pm\pi/8$ from the one-exciton band. This can be understood as follows. In the Frenkel exciton model, the oscillator strength for a particular state in the hexadecamer ring can be calculated from[8]

$$A = \sum_{mn} M_{mn}\psi^*(m)\,\psi(n) \quad (4.2)$$

where $\psi(m)$ labels the wave function, and for an in-plane head-to-tail transition-dipole configuration with circular symmetry the dipole-configuration matrix M_{mn} has a form

$$M_{mn} \equiv \mathbf{d}_m \cdot \mathbf{d}_n = \cos\left[(m-n)\frac{\pi}{8}\right] \quad (4.3)$$

It is easily verified that the above M_{mn} matrix has only 2 eigenstates with nonzero eigenvalues (both equal to 8). The corresponding eigenvectors $\phi_\pm(n)$ are

$$\phi_\pm(n) = \frac{1}{\sqrt{N}} e^{\pm in\pi/8} \quad (4.4)$$

One may flip the transition dipoles of the eight monomers in the upper half of the ring so that the resulting M_{mn} will acquire a minus sign if m and n belong to different half-rings:

$$\begin{aligned} A_{\text{flip}} &= \Big(\sum_{m,n=1}^{8} + \sum_{m,n=9}^{16} - \sum_{m=1}^{8}\sum_{n=9}^{16} - \sum_{n=1}^{8}\sum_{m=9}^{16}\Big) M_{mn}\psi^*(m)\,\psi(n) \\ &= A - 2\sum_{m=1}^{8}\sum_{n=9}^{16} M_{mn}\psi^*(m)\,\psi(n) - \\ &\qquad 2\sum_{m=9}^{16}\sum_{n=1}^{8} M_{mn}\psi^*(m)\,\psi(n) \quad (4.5) \end{aligned}$$

This results in dipole-allowed transitions from the zero-exciton ground state to one-exciton excited states with crystal momenta $k = 0, \pm\pi/4, \pm\pi/2, \pm 3\pi/4$. The previous allowed $k = \pm\pi/8$ states, however, are no longer optically bright in this transition-dipole configuration. The oscillator strengths for $k = 0, \pm\pi/4$ are 6.57 and 3.69, respectively. The ratio of oscillator strengths between the two energy levels ($k = 0$ and $k = \pm\pi/4$) equals 0.89. This agrees well with the ratio of oscillator strengths 0.88 from the INDO/S-LDM calculations, which can be easily extracted from Figure 7 by adding the values from the two panels at these two energies.

To compare with the absorption spectra from the INDO/S-LDM method with external fields pointing along two perpendicular in-plane directions, as shown in the two panels of Figure 7, one can write the transition dipole from the ground state $|0\rangle$ to the one-exciton state $|k\rangle$ in the form

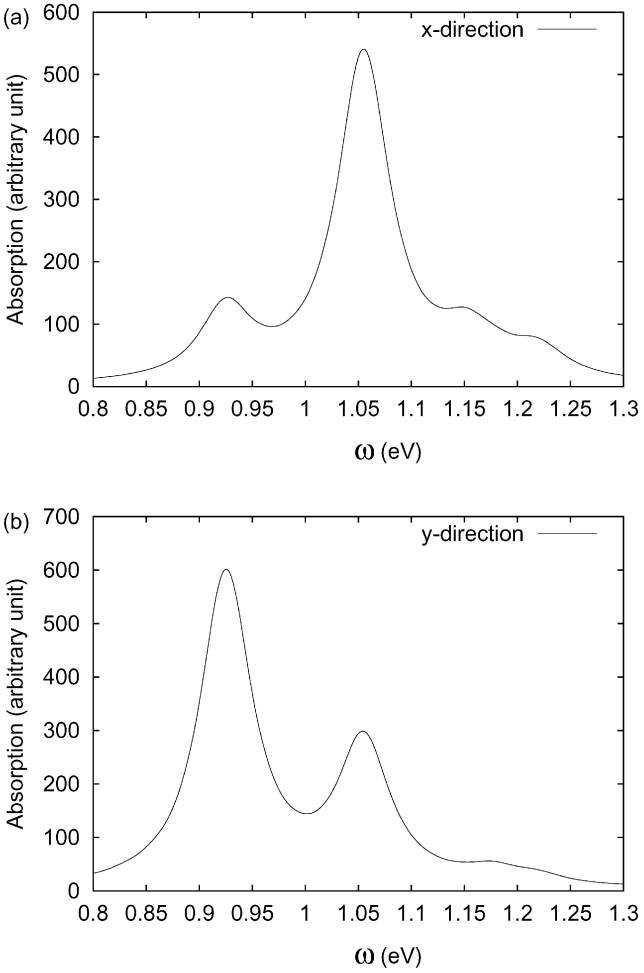

Figure 7. Absorption spectra from the INDO/S-LDM method with the upper 8 (above the *x*-axis) transition dipoles flipped and an applied external field pointing along two perpendicular in-plane directions: (a) *x* direction; (b) *y* direction.

$$\vec{\mu}_k = \langle 0|\sum_n \vec{\mu}_n(B_n^\dagger + B_n)|k\rangle \quad (4.6)$$

We note that eq 4.2 for calculating the oscillator strength A follows directly from eq 4.6. For a hypothetical in-plane head-to-tail transition-dipole configuration, we have

$$\vec{\mu}_k = 2\mu_0(\delta_{k,\pi/8} + \delta_{k,-\pi/8})\mathbf{e}_x - i2\mu_0(\delta_{k,\pi/8} - \delta_{k,-\pi/8})\mathbf{e}_y \quad (4.7)$$

Therefore, for the head-to-tail transition-dipole configuration absorption spectra are identical when the external field is pointing at *x* or *y* directions. However, if the individual transition dipoles of the eight monomers in the upper half of the ring are flipped, the combined transition dipole will be

$$\begin{aligned} \mathbf{e}_x\cdot\vec{\mu}_k &= 2\mu_0(-0.1656 + i0.3999)\delta_{k,\pi/4} + 2\mu_0(-0.1656 - \\ &\quad i0.3999)\delta_{k,-\pi/4} + 2\mu_0(-0.1327 + i0.1327)\delta_{k,\pi/2} + \\ &\quad 2\mu_0(-0.1327 - i0.1327)\delta_{k,-\pi/2} + 2\mu_0(-0.1283 + \\ &\quad i0.0532)\delta_{k,3\pi/4} + 2\mu_0(-0.1283 - i0.0532)\delta_{k,-3\pi/4} \\ \mathbf{e}_y\cdot\vec{\mu}_k &= 2\mu_0 0.64072\delta_{k,0} + 2\mu_0(-0.1920 + i0.0795)\delta_{k,\pi/4} + \\ &\quad 2\mu_0(-0.1920 - i0.0795)\delta_{k,-\pi/4} + 2\mu_0(-0.0264 - \\ &\quad i0.0264)\delta_{k,\pi/2} + 2\mu_0(-0.0264 + i0.0264)\delta_{k,-\pi/2} + \\ &\quad 2\mu_0(-0.0044 + i0.0106)\delta_{k,3\pi/4} + 2\mu_0(-0.0044 - \\ &\quad i0.0106)\delta_{k,-3\pi/4} \quad (4.8) \end{aligned}$$

TABLE 2: Q_y and Q_x Excitation Energies for the Two Different Dimers in the B850 Ring

dimer	Q_y (eV)	Q_x (eV)
1α−1β	1.08 Q_{y1}	1.98 Q_{x1}
	1.21 Q_{y2}	2.15 Q_{x2}
1β−2α	1.09 Q_{y1}	1.91 Q_{x1}
	1.21 Q_{y2}	2.17 Q_{x2}

TABLE 3: Spectrum of the Entire B850 Ring Calculated by the INDO/S-LDM Method in an Isolated State

lower band (cm^{-1})		upper band (cm^{-1})	
$k = 0$	7468.87	$k = 4\pi/8$	9501.44
$k = \pm\pi/8$	7904.43	$k = \pm5\pi/8$	9662.76
$k = \pm2\pi/8$	8517.42	$k = \pm6\pi/8$	9840.28
$k = \pm3\pi/8$	8985.23	$k = \pm7\pi/8$	9920.86
$k = -4\pi/8$	9259.47	$k = \pi$	9977.32

The x component of the absorption spectra should have zero $k = 0$ contribution if the transition dipoles obey strict tangential symmetry. In the INDO/S-LDM calculations, the transition dipoles of the BChls-a in the LH2 ring deviate from the ideal tangential configuration, and as a result, a small contribution from $k = 0$ appears in the x component. The ratio between the x and y components of the combined transition dipole is estimated to be between 2.20 (connecting Mg and N atoms) and 2.37 (connecting two N atoms), in agreement with the calculated spectra of the LH2 ring from which the ratio of the oscillator strengths along the x and y directions is found to be 5.14 (cf. Figure 7, the square root of 5.14 is 2.27, comparable to the estimated transition dipole ratio).

As we have demonstrated, the flipping of the transition dipoles of the eight monomers in the upper half of the ring can cause dipole-allowed transitions to $k = 0, \pm\pi/4, \pm\pi/2, \pm3\pi/4$. Similar techniques can be applied to find out other symmetry forbidden transitions. For example, one may flip the transition dipoles of the even-numbered monomers in the B850 ring to obtain optical transitions to $k = \pm7\pi/8$ state. In addition, one may also obtain transitions to $k = \pm3\pi/8, \pm5\pi/8$ states by multiplying a factor $\cos(\pi/2 \cdot n)$ (where n runs from 1 to 16) in eq 6, whereas a factor of $\cos(7\pi/8 \cdot n)$ is used for the $k = \pi$ state. Combined with the case with no transition-dipole flipping ($k = \pm\pi/8$), the complete spectrum of the B850 ring was resolved and results are displayed in Table 3.

V. Frenkel Exciton Model

The Frenkel exciton model was proposed to account for the Q_y excitation in the B850 ring. This approach has been applied for other systems such as phenylacetylene dendrimers, naphthalene dimers,[50] and the *Rhodopseudomoas (Rps.) acidophila* LH2 complex.[51] There were also suggestions of the existence of charge transfer states in light-harvesting systems.[52,53] To justify that the exciton is mainly localized in one BChl-a molecule only, we analyze the induced density matrices of the 1α−1β dimer at its Q_y excited state to study the extent of the intermonomer charge transfer states. From the density matrices, we calculate for the first two excitations a quantity p^ν defined as

$$p^\nu \equiv \frac{\sum_{ij}^{\text{intermonomer}} |\delta\rho_{ij}^\nu|^2}{\sum_{ij} |\delta\rho_{ij}^\nu|^2} \tag{5.1}$$

TABLE 4: ρ^ν Values for the First Two Excitations of the 1α−1β Dimer

1α−1β dimer	excitation ν (eV)	ρ^ν
Q_{y1}	1.08	0.024
Q_{y2}	1.21	0.020

where $\delta\rho_{ij}$ is the field-induced perturbation of the reduced density matrix element (linking orbital i and j) away from its ground-state value $\rho_{ij}^{(0)}$. The sum in the numerator is over the intermonomer components whereas the sum in the denominator is over all pairs of orbital i and j. The calculated values are presented in Table 4. The fact that p^ν is small implies that the excitation is predominantly a Frenkel exciton. From Table 4, for both Q_{y1} and Q_{y2} excitations, p^ν is 2%.

A crude excitonic model for a dimerized LH2 ring incorporating only nearest-neighbor interactions reads

$$\hat{H} = \sum_n (\epsilon_1 B_{2n}^\dagger B_{2n} + \epsilon_2 B_{2n+1}^\dagger B_{2n+1}) - \sum_n [B_{2n+1}^\dagger (J_1 B_{2n} + J_2 B_{2n+2}) + \text{c.c.}] \tag{5.2}$$

A 16 × 16 matrix representing the Hamiltonian of a ring of identical monomers with energies $\epsilon_1 = \epsilon_2 = \epsilon$ and alternating nearest-neighbor interactions (J_1 and J_2) can be diagonalized, yielding a set of eigenvalues, namely, 4 nondegenerate levels representing band edges ($\epsilon - J_1 - J_2$, $\epsilon + J_1 + J_2$, $\epsilon + J_1 - J_2$, and $\epsilon - J_1 + J_2$), and 6 doubly degenerate levels ($\epsilon \pm \sqrt{J_1^2+J_2^2}$, $\epsilon \pm \sqrt{J_1^2+J_2^2-\sqrt{2}J_1J_2}$, and $\epsilon \pm \sqrt{J_1^2 + J_2^2 + \sqrt{2}J_1J_2}$). The two nondegenerate states with energies $\epsilon - J_1 + J_2$ and $\epsilon + J_1 - J_2$ replace the doubly degenerate states with an energy ϵ in a homogeneous ring with $J_1 = J_2 = J$. If we put back the monomer energy inhomogeneity within the αβ-heterodimers ($\epsilon_1 \neq \epsilon_2$), the two-band structure will take the shape:

$$E_k = \frac{1}{2}(\epsilon_1 + \epsilon_2) \pm \sqrt{\frac{1}{4}(\epsilon_1 - \epsilon_2)^2 + J_1^2 + J_2^2 + 2J_1J_2 \cos 2k} \tag{5.3}$$

where ϵ_1 and ϵ_2 are the energies for the two monomers in a αβ-heterodimer, and $k = 0, \pm\pi/8, \pm\pi/4, ..., \pi$. We found that this simple exciton model cannot fit accurately the calculated low-lying excited-state energies in the B850 ring. A more general exciton model is required.

Schulten and co-worker[3,26] proposed a more realistic Hamiltonian of the hexadecamer,

$$\hat{H} = \begin{pmatrix} \epsilon_1 & J_1 & W_{1,3} & W_{1,4} & \cdot & & W_{1,2N-1} & J_2 \\ J_1 & \epsilon_2 & J_2 & W_{2,4} & \cdot & & \cdot & W_{2,2N} \\ W_{3,1} & J_2 & \epsilon_1 & \cdot & \cdot & & \cdot & \cdot \\ W_{4,1} & W_{4,2} & \cdot & \cdot & \cdot & & \cdot & \cdot \\ \cdot & \cdot & \cdot & \cdot & \epsilon_2 & & J_2 & W_{2N-2,2N} \\ \cdot & \cdot & \cdot & \cdot & J_2 & & \epsilon_1 & J_1 \\ J_2 & \cdot & \cdot & \cdot & W_{2N,2N-2} & & J_1 & \epsilon_2 \end{pmatrix} \tag{5.4}$$

where ϵ_1 and ϵ_2 are the excitation energies of the Q_y state of an individual BChl-a, J_1 and J_2 are the coupling constants between the nearest-neighbors of the entire ring, and N equals 8 as the system is of C_8 symmetry. In addition to the nearest-neighbor interactions J_1 and J_2, BChls-a that are not nearest-neighbors are coupled to each other via dipole−dipole interactions. The matrix $W_{i,j}$ in eq 5.4 is to add dipolar couplings to nonnearest neighbors:

$$W_{i,j} = C\left[\frac{\mathbf{d}_i\cdot\mathbf{d}_j}{|\mathbf{r}_{ij}|^3} - \frac{(\mathbf{d}_i\cdot\mathbf{r}_{ij})(\mathbf{d}_j\cdot\mathbf{r}_{ij})}{|\mathbf{r}_{ij}|^5}\right] \tag{5.5}$$

where the factor C is the proportionality constant to be determined, and $\boldsymbol{r}_{ij}$ is the vector connecting the ith and jth monomer. The direction of the transition dipole of the ith BChl-a is represented by a unit vector $\mathbf{d}_i$.

We first consider the dimer case. The electronic J couplings are computed from

$$4J_i^2 = \Delta E_i^2 - \Delta\epsilon^2 \qquad i = 1, 2 \tag{5.6}$$

where $\Delta\epsilon = \epsilon_1 - \epsilon_2$ is the difference between the two monomers' Q_y excitation energies, J_1 (J_2) is the intermonomer coupling of the 1α−1β (1β−2α) dimer, and ΔE_i is the splitting of the eigenvalues of the matrices

$$\begin{pmatrix}\epsilon_1 & J_1\\ J_1 & \epsilon_2\end{pmatrix} \quad \text{and} \quad \begin{pmatrix}\epsilon_2 & J_2\\ J_2 & \epsilon_1\end{pmatrix} \tag{5.7}$$

From eq 5.6, the J values calculated are shown in Table 5. These are the values based on the Frenkel exciton model where intermonomer charge transfer is not considered.

To determine the J values of the complete B850 ring, one can fit eq 5.4 by a Monte Carlo procedure. An initial guess of the parameters in eq 5.4 is made, and the 16 × 16 matrix is diagonalized resulting in 16 eigenstates. As the system is dimerized, we use the capital K (instead of k) to label the states here. $K = 0$ and $K = \pi$ states are nondegenerate, and $K = \pm\pi/4$, $\pm 2\pi/4$ and $\pm 3\pi/4$ are doubly degenerate. The energy for each K state is compared with the corresponding energy from the INDO/S-LDM spectra, and the difference is used to calculate the root-mean-square (rms) error for that particular iteration step. The process is repeated until a desired precision is reached. ϵ_1 is assumed to be greater than ϵ_2, and they are constrained so that the sum of diagonal elements in eq 5.4 is equal to the sum of the calculated INDO/S-LDM energies, i.e.,

$$8(\epsilon_1 + \epsilon_2) = \sum_i E_i \tag{5.8}$$

where E_i is the energy of the ith INDO/S-LDM state. We present our result in Figure 8a. The total rms error is about 118 cm^{-1}. The final J_1, J_2, ϵ_1, ϵ_2 and C values are presented in Table 6.

Only two calculations of the entire B850 ring have been reported in the literature, and both used the INDO/S-CIS method.[3,26] The spectra of the B850 ring calculated via INDO/S-LDM and those via INDO/S-CIS are compared in Figure 8. In Figure 8a, the LDM result is represented by crosses, and the fitting result by pluses. In Figure 8b the CIS result is shown by crosses and the fitting result, by pluses. Note that the INDO/S-CIS method fitted the band edges, i.e., the $K = 0$ and $K = \pm\pi$ states, whereas LDM fitted the complete 10 energy levels. The fitting result in Figure 8a is better in the sense that a smaller rms error (118 cm^{-1}) is achieved (compared with a rms of 258 cm^{-1} in INDO/S-CIS method).

From the B850 ring fitting (cf. Table 6), we note that both ϵ_1 and ϵ_2 become smaller and their difference vanishes. The reason can be analyzed by calculating the ground-state dipolar field acting on a specific α-BChl-a or a β-BChl-a due to its nonnearest-neighbors. To calculate the dipole fields, we employ

$$\mathbf{E}(\boldsymbol{x}) = \frac{3\mathbf{n}(\mathbf{p}\cdot\mathbf{n}) - \mathbf{p}}{|\mathbf{x} - \mathbf{x}_0|^3} \tag{5.9}$$

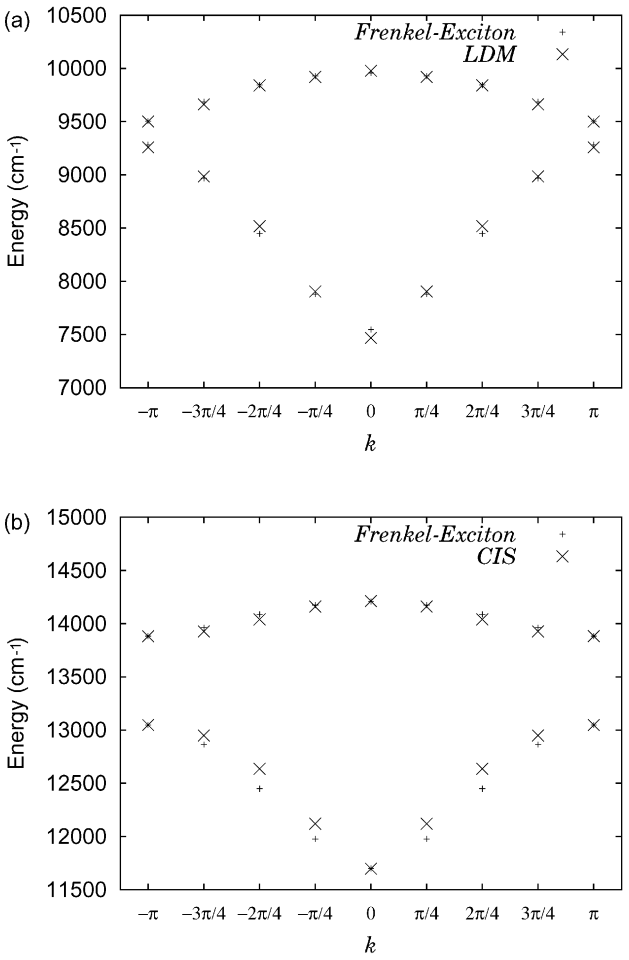

Figure 8. (a) Ten energy levels extracted from the absorption spectra (cross), and correspondingly fitted ten eigenvalues from a dimerized Hamiltonian with additional dipolar interactions between non-nearest BChl-a neighbors (plus); the fitting parameters are $J_1 = 593.9$ cm^{-1}, $J_2 = 490.6$ cm^{-1}, $\epsilon_1 = 9116.9$ cm^{-1}, $\epsilon_2 = 9116.7$ cm^{-1}, and $C = 640725$ Å^3 cm^{-1}. The x-axis is labeled by the crystal momenta of the exciton $p = \pm K\pi/4$. (b) Excitation energies calculated by the INDO/S-CIS method and their fittings.

TABLE 5: Calculated *J* Coupling Constants (cm^{-1}) for the Two Dimers in the B850 Ring

	methods				
	LDM dimer	LDM ring	CEO dimer	ZINDO ring	PDA dimer
1α−1β	528	594	408	790	339
1β−2α	455	491	366	369	336

TABLE 6: Fitting Parameters for the B850 Ring

	J_1	J_2	ϵ_1	ϵ_2	C/Å^3	rms
B850 ring	593.9	490.6	9116.9	9116.7	640725	118

where $\mathbf{E}$ is the dipole field at a point $\mathbf{x}$ due to a ground-state dipole $\mathbf{p}$ at the point $\mathbf{x}_0$ and $\mathbf{n}$ is a unit vector connecting $\mathbf{x}$ and $\mathbf{x}_0$. A summation is carried out for the dipole effect acting on an α-BChl-a and a β-BChl-a, respectively. The summations of dipoles acting on the α-BChl-a and β-BChl-a are estimated to be 8.0×10^{-4} and 9.8×10^{-4} Å^{-2}, respectively. The energy E is calculated by

$$E = -\mathbf{E}\cdot\vec{\mathbf{d}} \tag{5.10}$$

where $\vec{d}$ is the transition dipole for that particular α- and β-BChls-a. As a result, the energies acting on the α- and β-BChls-a due to the ground-state dipole of the rest of BChls-a

in the B850 ring except its nearest-neighbor are −194 and −153 cm^{-1}, respectively. We can thus determine the net effect of the field dipole of the rest of the BChls-a acting on the α-BChl-a is larger than that on the β-BChl-a. This helps to explain qualitatively why the ϵ_1 and ϵ_2 values of the B850 ring have a vanishing difference. J_1 and J_2 determined from the INDO/S-CIS calculations on the B850 ring[3,26] are very different from those from the dimer calculations. J_1 and J_2 fitted from the INDO/S-LDM calculation of the B850 ring are similar to those from the INDO/S-LDM dimer calculation. The INDO/S-LDM calculations here thus resolve the long-existing discrepancy. The fact that the J_1 and J_2 values in Table 6 are larger than those in refs 24, 25, and 7 can be attributed to long-range dipolar interactions in the ring and our INDO/S parametrization.

To further justify the value of C, we have calculated the transition dipole moment of the monomer Q_y state. The transition dipole moment is calculated by the formula[24]

$$\mu^{\nu} = \mathrm{Tr}(\delta\rho_{ij}^{\nu}\cdot\mu_{ij}) \tag{5.11}$$

where μ^{ν} is the transition dipole at excitation ν, and μ_{ij} is the dipole moment operator, $\delta\rho_{ij}^{\nu}$ is the induced density matrix at excitation ν obtained from a Fourier transform,

$$\delta\rho(\omega) = \int \mathrm{d}t\, \exp^{\mathrm{i}\omega t}\, \delta\rho(t) \tag{5.12}$$

where ω is the excited-state frequency, $\delta\rho(\omega)$ and $\delta\rho(t)$ are the frequency-domain and time-domain induced density matrices when $|\mathbf{E}| = 1$ V/Å, respectively. The normalized frequency domain induced density matrix takes the form $(\mathrm{Im}(\delta\rho(\omega)) + \mathrm{Im}(\delta\rho^{\mathrm{T}}(\omega)))/\mathrm{i}\sqrt{2})$, where $\delta\rho^{\mathrm{T}}(\omega)$ is the transpose of $\delta\rho(\omega)$. The transition dipole moment is calculated to be 2.326 e Å. Based on eq 5.5, a relation between the transition dipole moment and the C value is established:

$$\mu^2 \times 1.16 \times 10^5 = C \tag{5.13}$$

from which we obtain $C = 639765$ $Å^3$ cm^{-1}. This is consistent with the fitting result for the entire B850 ring (640725 $Å^3$ cm^{-1}).

VI. Solvent Effect

In this section we take into account solvent effects for monomers and dimers using the Onsager solvation model with the self-consistent reaction field (SCRF) treatment.[26,54,55] In isolated-state calculations, the dimeric J_1 and J_2 coupling constants are determined spectroscopically, i.e., from the energy splitting of the Q_y state in the spectrum. To account for the solvent effect on the coupling constants J_1 and J_2, we cannot determine it spectroscopically together with the Onsager model because this is a PDA model. Instead, another method based on the Q_y density matrix of monomers is adopted to calculate the J coupling constants in a solvent.

A. Monomer. Taking the α-BChl-a as an example, the solvent effect is calculated by modifying the ground-state Fock operator by adding the Onsager dipolar term,[54,55]

$$F_{mn} = F_{mn}^{0} - \frac{2(\epsilon-1)}{2\epsilon+1}\frac{\vec{\mu}_{\mathrm{g}}\cdot\vec{\mu}_{mn}}{{a_0}^3} \tag{6.1}$$

where F_{mn} is the modified Fock operator, F_{mn}^{0} is the Fock operator in the absence of the solvent effect, $\vec{\mu}_{\mathrm{g}}$ is the ground-state dipole moment, $\vec{\mu}_{mn}$ is the dipole integral, ϵ is the dielectric constant, which is equal to 9,[56] and a_0 is the cavity radius, which is estimated to be 5.75 Å by the Gaussian 98 package[57] at the ab initio 6-31+G* Hartree−Fock level. The calculated ground-state dipole moment is shifted from 7.7 to 22.0 D. Similar results were obtained by others.[25,26] In ref 25, it was reported that the shift was from 6.8 to 20.5 D whereas in ref 26, 7.3 to 21 D.

TABLE 7: Calculated Dimer J Coupling Constants (cm^{-1}) Using Both the Spectroscopic and Coulombic Methods

	1α−1β	1β−2α
spectroscopic method (isolated state)	528	455
Coulomb method (isolated state)	434	364
Coulomb method (dielectric medium)	322	273

For the excited state, the Hamiltonian term due to interactions with the external fields is modified.

$$\hat{H}_{ext} = -\mathbf{E}\cdot(\hat{\vec{\mu}}_g + \hat{\vec{\delta\mu}}) - [\frac{(D'-1)}{2D'+1} + (\frac{2(\eta^2-1)}{2\eta^2+1})]\hat{\vec{\mu}}_g\cdot\hat{\vec{\delta\mu}} \tag{6.2}$$

where $\vec{\mu}_{\mathrm{g}}$ is the ground-state dipole moment, $\delta\vec{\mu}$ is the field-induced dipole moment, η is the index of refraction ($\eta = 1.6$), and D' is the contribution to the bulk dielectric due to orientation ($D' = 1.7465$). The solvent effect on the monomer is larger for the Q_y excitation than for the Q_x excitation. The Q_y peak is shifted from 1.17 to 1.42 eV whereas the Q_x peak remains at about 2.15 eV (experimentally, the peaks are found at 1.6 and 2.16 eV for the Q_y and Q_x excitations, respectively[58]). Table 1 summarizes the excitation energies of the three monomers in comparison with the experimental values. Values inside the parentheses include solvent effects.

B. J_1 and J_2 Coupling Constants. Next, we examine the solvent effect on the dimeric coupling constants using a method by Tretiak et al. that neglected the electron exchange interaction.[25] The coupling constants calculated so far are spectroscopic in nature (estimated from the Davydov splitting in the spectrum[25]). Here we adopt an alternative approach based on Coulombic interactions. The Coulombic coupling J_{AB} between monomers A and B are calculated from[25]

$$J_{\mathrm{AB}} = \sum_{n\in\mathrm{A},m\in\mathrm{B}} V_{nm}(\delta\rho_{\nu}^{\mathrm{A}})_{nn}(\delta\rho_{\nu}^{\mathrm{B}})_{mm} \tag{6.3}$$

where $(\delta\rho_{\nu}^{\mathrm{A}})_{nn}$ and $(\delta\rho_{\nu}^{\mathrm{B}})_{mm}$ are the diagonal parts of the density matrix variation at frequency ν of monomers A and B, respectively. V_{nm} is the INDO/S Coulombic two-electron integrals corresponding to the AB dimer pair. This Coulombic expression allows determination of the J coupling by the Q_y density matrix variation of each monomer both for the isolated dimers and for dimers in a dielectric medium.

We compare the spectroscopic method and the Coulombic method for calculating the dimer J values in the isolated state. In Table 7, we estimate J_1 and J_2 to be 528 and 455 cm^{-1} by the spectroscopic method, respectively, and 434 and 364 cm^{-1} by the Coulombic method, respectively. The differences of the J values from the two methods are attributed to the short-range exchange interactions.[25,59−61] The reduction of J_1 and J_2 are about 17% and 20%, respectively (11% and 13% are reported in ref 25, respectively).

We employ the Coulombic method to account for the solvent effect for the dimer coupling constants. J_1 and J_2 for isolated state (dielectric medium) are 434 cm^{-1} (322 cm^{-1}) and 364 cm^{-1} (273 cm^{-1}), respectively (cf. Table 7). A reduction of about 25% for each J. The J values become smaller in dielectric

media. It may be attributed to the fact that the transition dipole moment of the monomer decreases in a solvent. The transition dipole of the Q_y state of the α-BChl-a is found to be 2.326 *e* Å (2.067 *e* Å) in an isolated state (a dielectric medium). Note that the reduction is about 12%, in agreement with a reduction of 15−20% reported in ref 25.

The *J* coupling constants of the B850 ring have been determined using the LDM-INDO/S method, and J_1 and J_2 are found to be 594 cm^{-1} and 491 cm^{-1}, respectively. We determine that the solvent effect brings the dimer *J* coupling constants down by about 25%. A rough estimation is applied to the B850 ring. As a result, J_1 and J_2 are estimated to be 445 cm^{-1} and 367 cm^{-1} after taking into account of the solvent effects.

VII. Conclusions

The INDO/S-LDM method is employed to calculate electronic structures of the B800 and B850 rings of *Rs. molischianum*. As all valence electrons are included explicitly in the calculation for the system containing 736 atoms and 2176 orbitals (the B850 ring), it is demonstrated that the INDO/S-LDM method is well-suited for calculations of electronic structures of very large systems. Note that all calculations are performed on a PC 700 MHz machine with 512 MB memory. Adequate accuracy has been achieved. The INDO/S-LDM method demonstrates directly that the J_1 and J_2 values of the complete B850 ring are similar to those derived from the dimer calculation. This resolves a long-existing discrepancy in the field and reveals that the electron−hole pair is mainly localized in one BChl-a with slight leakages to its nearest-neighbors. The excellent fit between the parametrized long-range dipolar Frenkel exciton model and the calculated low-lying LDM-INDO/S excited-state energies of the B850 ring provides strong support to the Frenkel exciton description of the photoexcitations in the B850 ring. Taking into account of the solvent effects, the calculated J_1 and J_2 values for the B850 ring are consistent with the estimated values reported in the literature.

Further studies of the LH2 can make improvements in several areas. For instance, the time-dependent density functional theory (TDDFT)[62] may be employed to verify the Frenkel exciton model and to examine its parameters. Moreover, solving the entire B850 ring including the solvent effect can result in much more accurate estimations of J_1 and J_2 coupling constants and excitation energies. An explicit solvent model is desirable. This requires much more computational resources, and simulations can be carried out by implementing the INDO/S-LDM method on parallel machines.

Acknowledgment. Support from the Hong Kong Research Grant Council (RGC) and the Committee for Research and Conference Grants (CRCG) of the University of Hong Kong is gratefully acknowledged. We thank Dr. S. Yokojima and Dr. W. Z. Liang for making the LDM codes available for all these calculations.

References and Notes

(1) McDermott, G.; Prince, S. M.; Freer, A. A.; Hawthornthwaite-Lawless, A. M.; Papiz, M. Z.; Cogdell, R. J.; Isaacs, N. W. *Nature* **1995**, *374*, 517.

(2) Koepke, J.; Hu, X.; Muenke, C.; Schulten, K.; Michel, H. *Structure* **1996**, *4*, 581.

(3) Hu, X.; Ritz, T.; Damjanovic, A.; Schulten, K. *J. Phys. Chem. B* **1997**, *101*, 3854.

(4) Förster, Th. *Naturwissenschaften* **1946**, *33*, 166.

(5) Hess, S.; Visscher, K. J.; Pullerits, T.; Sundström, V. *Biochemistry* **1994**, *33*, 8300,

(6) Davydov, A. S. *Theory of Molecular Excitons*; Plenum Press: New York, 1971.

(7) Sundström, V.; Pullerits, T.; van Grondelle, R. *J. Chem. Phys. B* **1999**, *103*, 2327.

(8) Meier, T.; Zhao, Y.; Chernyak, V.; Mukamel, S. *J. Chem. Phys*. **1997**, *107*, 3876.

(9) Zhao, Y.; Meier, T.; Zhang, W. M.; Chernyak, V.; Mukamel, S. *J. Phys. Chem. B* **1999**, *103*, 3954.

(10) Dahlbom, M.; Beenken, W.; Sundström, V.; Pullerits, T. *Chem. Phys. Lett*. **2002**, *364*, 556.

(11) Meier, T.; Chernyak, V.; Mukamel, S. *J. Phys. Chem. B* **1997**, *101*, 7332. Zhang, W. M.; Meier, T.; Chenyak, V.; Mukamel, S. *J. Chem. Phys*. **1998**, *108*, 7763.

(12) Leegwater, J. A. *J. Chem. Phys*. **1996**, *100*, 14403.

(13) Pullerits, T.; Chachisvilis, M.; Sundström, V. *J. Chem. Phys*. **1996**, *100*, 10787.

(14) Monshouwer, R.; Abrahamsson, M.; van Mourik, F.; van Grondelle, R. *J. Phys. Chem. B* **1997**, *101*, 7241.

(15) Ray, J.; Makri, N. *J. Phys. Chem. A* **1999**, *103*, 9417.

(16) Dahlbom, M.; Pullerits, T.; Mukamel, S.; Sundström, V. *J. Phys. Chem. B* **1999**, *105*, 9418.

(17) Leupold, D.; Stiel, H.; Teuchner, K.; Nowak, F.; Sandner, W.; Ücker, B.; Scheer, H. *Phys. Rev. Lett*. **1996**, *77*, 4675.

(18) Chacisvilis, M.; Kühn, O.; Pullerits, T.; Sundström, V. *J. Phys. Chem. B* **1997**, *101*, 7275.

(19) Novoderezhkin, V.; Monshouwer, R.; van Goundelle, R. *Biophys. J*. **1999**, *77*, 666.

(20) Kühn, O.; Sundström, V.; Pullerits, T. *Chem. Phys*. **2002**, *275*, 15.

(21) Redfield, A. G. *Adv. Magn. Reson*. **1965**, *1*, 1.

(22) Gouterman, M. *J. Mol. Spectrosc*. **1961**, *6*, 138.

(23) Weiss, C. *J. Mol. Spectrosc*. **1972**, *44*, 37.

(24) Tretiak, S.; Chernyak, V.; Mukamel, S. *J. Phys. Chem. B* **2000**, *104*, 4519.

(25) Tretiak, S.; Middleton, C.; Chernyak, V.; Mukamel, S. *J. Phys. Chem. B* **2000**, *104*, 9540.

(26) Cory, M. G.; Zerner, M. C.; Hu, X.; Schulten, K. *J. Phys. Chem. B* **1998**, *102*, 7640.

(27) Takahashi, A.; Mukamel, S. *J. Chem. Phys*. **1994**, *100*, 2366.

(28) Fukutome, H. *J. Mol. Struct. (THEOCHEM)* **1989**, *188*, 337.

(29) Soos, Z. G.; Ramasesha, S.; Galvo, D. S.; Etemad, S. *Phys. Rev. B* **1993**, *47*, 1742.

(30) Liang, W. Z.; Yokojima, S.; Zhou, D. H.; Chen, G. H. *J. Phys. Chem. A* **2000**, *104*, 2445.

(31) Liang, W. Z.; Wang, X. J.; Yokojima, S.; Chen, G. H. *J. Am. Chem. Soc*. **2000**, *122*, 11129.

(32) Liang, W. Z.; Yokojima, S.; Ng, M.-F.; Chen, G. H.; He, G. Z. *J. Am. Chem. Soc*. **2001**, *123*, 9830.

(33) Bacon, A. D.; Zerner, M. C. *Theor. Chim. Acta* **1979**, *53*, 21.

(34) Stewart, J. J. P. *J. Comput. Chem*. **1989**, *10*, 209; **1989**, *10*, 221.

(35) Pople, J. A.; Segal, G. A. *J. Chem. Phys*. **1965**, *43*, S136.

(36) Pople, J. A.; Beveridge, D. L.; Dobosh, P. *J. Chem. Phys*. **1967**, *47*, 2026.

(37) Ridley, J.; Zerner, M. C. *Theor. Chim. Acta* **1973**, *32*, 111.

(38) Yokojima, S.; Chen, G. H. *Phys. Rev. B* **1999**, *59*, 7259.

(39) Yokojima, S.; Chen, G. H. *Chem. Phys. Lett*. **1998**, *292*, 379.

(40) Tretiak, S.; Chernyak, V.; Mukamel, S. *Chem. Phys. Lett*. **1998**, *297*, 357.

(41) Edwards, L.; Dolphin, D. H.; Gouterman, M.; Adler, A. D. *J. Mol. Spectrosc*. **1971**, *38*, 16.

(42) Baker, J. D.; Zerner, M. C. *Chem. Phys. Lett*. **1990**, *175*, 192.

(43) Nakatsuji, H.; Hasegawa, J.; Hada, M. *J. Chem. Phys*. **1996**, *104*, 2321.

(44) Gwaltney, S. R.; Bartlett, R. J. *J. Chem. Phys*. **1998**, *108*, 6790.

(45) Beekman, L. M. P.; et al. *J. Chem. Phys. B* **1997**, *101*, 7293.

(46) Polívka, T.; et al. *J. Chem. Phys. B* **2002**, *106*, 11016.

(47) He, Z.; Sundström, V.; Pullerits, T. *Chem. Phys. Lett*. **2001**, *334*, 159.

(48) Kasha, M.; Rawls, H. R.; Ashraf El-Bayoumi, M. *Pure Appl. Chem*. **1965**, *11*, 371.

(49) Damjanović, A.; Vaswani, H. M.; Fromme, P.; Fleming, G. R. *J. Phys. Chem. B* **2002**, *106*, 10251.

(50) Poliakov, E.; Chernyak, V.; Tretiak, S.; Mukamel, S. *J. Chem. Phys*. **1999**, *110*, 8161. Minami, T.; Tretiak, S.; Chernyak, V.; Mukamel, S. *J. Lumin*. **2000**, *87*−*9*, 115.

(51) Linnanto, J.; Korppi-Tommola, J. E. I.; Helenius, V. M. *J. Phys. Chem. B* **1999**, *103*, 8739.

(52) Alden, R. G.; et al. *J. Chem. Phys. B* **1997**, *101*, 4667.

(53) Polívka, T.; Pullerits, T.; Herek, J. L.; Sundström, V. *J. Chem. Phys. B* **2000**, *104*, 1088.

(54) Karlsson, G.; Zerner, M. C. *Int. J. Quantum Chem*. **1973**, *7*, 35.

(55) Karelson, M. M.; Zerner, M. C. *J. Phys. Chem*. **1992**, *96*, 6949.

(56) King, G.; Lee, F.; Warshel, A. J. *J. Chem. Phys*. **1991**, *95*, 4366.

(57) Frisch, M. J.; Trucks, G. W.; Schlegel, H. B.; Scuseria, G. E.; Robb, M. A.; Cheeseman, J. R.; Zakrzewski, V. G.; Montgomery, J. A., Jr.; Stratmann, R. E.; Burant, J. C.; Dapprich, S.; Millam, J. M.; Daniels, A. D.; Kudin, K. N.; Strain, M. C.; Farkas, O.; Tomasi, J.; Barone, V.; Cossi, M.; Cammi, R.; Mennucci, B.; Pomelli, C.; Adamo, C.; Clifford, S.; Ochterski, J.; Petersson, G. A.; Ayala, P. Y.; Cui, Q.; Morokuma, K.; Malick, D. K.; Rabuck, A. D.; Raghavachari, K.; Foresman, J. B.; Cioslowski, J.; Ortiz, J. V.; Stefanov, B. B.; Liu, G.; Liashenko, A.; Piskorz, P.; Komaromi, I.; Gomperts, R.; Martin, R. L.; Fox, D. J.; Keith, T.; Al-Laham, M. A.; Peng, C. Y.; Nanayakkara, A.; Gonzalez, C.; Challacombe, M.; Gill, P. M. W.; Johnson, B. G.; Chen, W.; Wong, M. W.; Andres, J. L.; Head-Gordon, M.; Replogle, E. S.; Pople, J. A. *Gaussian98*, revision x.x; Gaussian, Inc.: Pittsburgh, PA, 1998.

(58) Oelze, J. *Methods Microbiol*. **1985**, *18*, 257.

(59) Krueger, B. P.; Scholes, G. D.; Fleming, G. R. *J. Phys. Chem. B* **1998**, *102*, 5378.

(60) Scholes, G. D.; Gould, I. R.; Cogdell, R. J.; Fleming, G. R. *J. Phys. Chem. B* **1999**, *103*, 2543.

(61) Timpmann, K.; et al. *J. Phys. Chem. B* **2001**, *105*, 8436.

(62) Runge, E.; Gross, E. K. U. *Phys. Rev. Lett*. **1984**, *52*, 997.